Australasian Universities Power Engineering Conference
M. Negnevitsky, ed., Hobart, Australia, September 25 - 28, 2005

A Parametric Finite Element Analysis Package for Electromagnetic Fields of Electrical Machine

Shuhong Wang[1,2], Jie Qiu[1], Qingfu Li[1]
[1]Faculty of Electrical Engineering
Xi'an Jiaotong University
Xi'an, Shaanxi, China
shwang@mail.xjtu.edu.cn

Jian Guo Zhu[2], Youguang Guo[2]
[2]Faculty of Engineering
University of Technology, Sydney
Sydney, NSW 2007, Australia
joe@eng.uts.edu.au

ABSTRACT

This paper develops a parametric finite element analysis package for the electromagnetic fields in electrical machines. Based on Petri net, a parametric finite element geometrical modelling method is presented, with which the user can interactively utilize variables to describe the dimensional and geometrical constraints. The efficiency of revision of finite element geometrical model is enhanced. An electromagnetic finite element adaptive mesh generation method based on fuzzy logic control is proposed, by which more appropriate mesh distribution can be obtained. A V-A model of switches is developed, which has been applied to the dynamic simulation of magnetic field coupled with drive circuits. Comparing the simulation results with the experimental observation, the satisfaction of this model is confirmed. The advantages of this package are its precision and flexibility. These will significantly make the user focus more on their individual physical problems.

1. INTRODUCTION

Finite element method (FEM) is favoured for its merits, especially, high precision and adaptability. Unfortunately, FEM often requires users to possess much knowledge of mathematics and handle a large amount of data. Therefore, a more friendly and practical package for finite element (FE) analysis is necessary. This paper aims to present a FEM package for the designers to analyse practical problems and also for students to construct and solve problems on their own in order to achieve deeper insight into electromagnetic phenomena.

This paper summarizes our previous work, aiming to introduce the development of this software package. The implementations of the three sections in the developed FE package, including parameterized FE geometric modelling [1], fuzzy control adaptive FE meshing [2], and field-circuit coupled computation based on a proposed switch model [3], are presented.

In many cases, a user may have to create and analyse families of similar devices to get the best results from a FE analysis package. The parameterized geometric modelling system can provide an environment to create a draft FE model defined by diverse variables, expressions and geometric constraints, and effectively change the FE geometric model by modification of some parameters. In particular, the shape or size optimization allows a repetitive modification of the geometric FE model. Some parametric electromagnetic FE environments have been developed by the ordered symbolic description [4] or the variational geometry method [5]. In this paper, Petri net is utilized to describe the parameterized geometric modelling of FE package.

There are two types of error estimation methods: one is based on the residual of differential equations, such as Z^2 *posteriori* error estimator; the other is based on boundary conditions of element interface. Four types of artificial intelligence (AI) techniques have been applied in FEM, including Knowledge-Based Expert Systems (KBES), Neural Networks (NN), Fuzzy Logic (FL), and Genetic Algorithms (GA). The intellectualized level of FEM software packages can be enhanced by using such AI techniques. In this paper, based on Z^2 *posteriori* error estimator, fuzzy control is applied in the adaptive FE meshing and an appropriate refinement factor can be calculated.

The performance of magnetic nonlinear devices can be modelled with good accuracy using numerical magnetic field analysis. However, these devices are usually components in a complex electric circuit. To perform a system simulation efficiently, a circuit simulator and a numerical magnetic field solver must be combined. One method is loose coupled, in which a finite element analysis yields lumped element values for the circuit. In nonlinear analysis, this method requires iteration between the field computation and the circuit package until both the circuit and fields are stable. Another method is tightly coupled, which integrates external circuit into FE system of equations. The advantage of the second method is avoiding iterative computation between FE and circuit, and saving the computation time. The total number of the FE-circuit coupled equations is only slightly larger than that of FE equations. The cost of solving a coupled system is not significantly increased compared to solving the FE system.

Since more and more electromagnetic devices are controlled by converters, the modelling of power electronic circuit become very important for field-circuit coupled computation. Good approaches should be: 1) to use the Modified Nodal Analysis (MNA) technique which is well suited to the requirements of digital computer programming; 2) to perform the simulation requiring no prior knowledge of the circuit operation, i.e. the circuit topology modification. In this paper, a new V-A characteristic of ideal switches is proposed, and the field-circuit coupled model based on this V-A characteristic is discussed.

2. PETRI NET-BASED PARAMETERIZED FE GEOMETRIC MODELLING

2.1. BRIEF INTRODUCTION OF PETRI NET

Petri net, originally proposed by Carl Adam Petri [1], is a directed, weighted graph consisting of four main types of graphical modelling elements, known as "place", "transition", "arc", and "token". A place, denoted as a circle or ellipse, represents a condition. A transition, depicted as a solid bar, represents an event. Arcs, with weight and arrows, are utilized to connect places and transitions. A place may contain zero or several tokens, drawn as small black dots. In general, each transition has its own "firing" condition, i.e. transition rule. For example, a transition t is enabled if each of its input places has at least one token, and then one token will be removed from each input place and be added to each output place. Figure 1 shows the schematic graph of a Petri net.

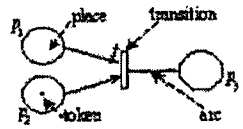

Figure 1: Schematic graph of a Petri net

2.2. PETRI NET-BASED DESCRIPTION OF PARAMETERIZED FE GEOMETRIC MODEL

In a parametric model, all the parameters are regarded as variables. The variables controlled by the designer are called independent variables, and the others are known as dependent variables. The graphic entities can be specified with dimensional and geometrical constraints. The dimensional constraints are described by expressions, composed of operators, variables and functions. The geometrical constraints consist of intersection, parallel, perpendicularity, and etc. A change in an independent variable's value will cause changes in dependent variables and hence entities according to their respective constraints.

The parameterized FE geometric modelling based on Petri net can be described as: $\Sigma=(S, T, F, W, M_0)$. There are two types of place in the place set S: geometry entities and variables. The capacity of each place is 1. Transition set T is composed of dimensional and geometrical constraints, which may be executed as an event. The arcs in the arc set F denote directions of parametric reasoning and the total arc weights in set W are 1. The initial tokens in set M_0 are depicted with dots. The initial token of independent places is 1 at the beginning of parametric reasoning. Figure 2 illustrates the parametric model of an example described as a Petri net.

2.3. CONSTRAINT REASONING STRATEGY DESCRIBED BY PETRI NET

A proposed constraint reasoning strategy is defined as a transition rule: a transition, which represents a constraint, is enabled when each of its input places contains one token and no output place has one. After the transition fires, the token of each output place becomes to 1. Because the dependent variables may also be regarded as other transitions' input places, in contrast to the traditional firing rule introduced in Section 2.1, the tokens in the input places of this transition still remain as 1. If each place in the model holds a token, the constraint reasoning procedure is completed. The variables are all defined and the entities are all redrawn. The parametric constraint reasoning cannot be accomplished if a constraint conflict occurs. If the total number of places, whose token is 0, does not change when constraint reasoning is made continuously twice, it is considered as that there exist some constraint conflicts.

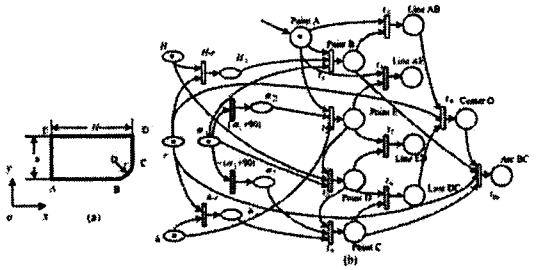

(a) An example (b) Petri net-based description

Figure 2: Parametric model described as Petri net

Petri net may clearly specify the automatic update of a parameterized FE geometric model, avoid the complexity of calculating the nonlinear equations for variational geometry, and easily find out conflict constraints. The reasoning cost is proportional to the number of constraints. The parametric constraint reasoning is independent of the constructing sequence of the variables and entities.

2.4. APPLICATION OF PETRI NET-BASED PARAMETERIZED FE GEOMETRIC MODELLING

The parametric modelling processes and FE meshing are applied in two similar rotor slots of two different induction motors. Figure 3 illustrates the cross-sectional diagram of the slot and its dimension variables. The independent and some dependent variables shown in Figure 3 are listed in Tables 1 and 2, respectively.

Because of the structural symmetry, the parametric model of half slot of type 1 is defined at first. Modifying the independent variables using data of type 2, the half slot of type 2 is acquired automatically by parametric constraint reasoning. Figure 4 shows the parametric modelling and reasoning process of the half slot. The FE meshes of the two type rotors are illustrated in Figure 5.

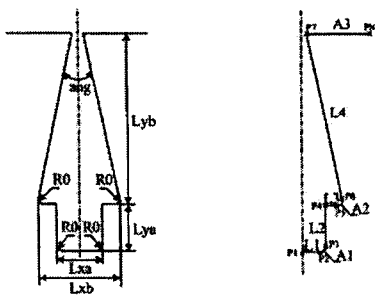

Figure 3: Representation of the trapezia slot of rotor

Table 1: Independent variables

Independent Variables	Type 1	Type 2
Lxa (mm)	10.06	8
Lxb (mm)	13.06	10.3
Lya (mm)	10	8
Lyb (mm)	44	33
R0 (mm)	0.5	0.5
R(mm) : Outer radius of rotor	307.8	170.2
ang (°)	14	14
N : Slot Number	47	50

Table 2: Some dependent variables

Some Dependent Variables	Expression
Length of line L1	0.5*Lxa-R0
Length of line L2	Lya-R0
Length of line L3	0.5*(Lxb-Lxa)-R0
Length of line L4	(Lyb-R0*sin(45+Ang/4))/cos(Ang/2)

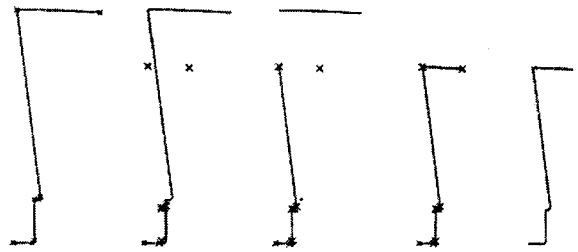

Figure 4: Parametric modelling process

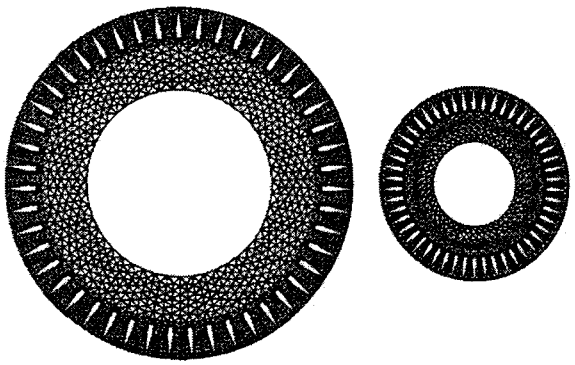

(a) Type 1 (b) Type 2

Figure 5: FE meshes of two rotors

3. Fuzzy Control Adaptive FE Mesh Generation

3.1. Mesh Generation

By combining the advancing front method and Delaunay triangulation approach, a FE mesh generation is described as follows: 1) Discretize the boundary and place nodes on the boundary. The node can be regarded as the center of a circle, the so-called "coin"; 2) Connect all nodes along the boundary to make a closed counter-clockwise chain, called advancing front node-chain; 3) Generate a new node. Figure 6 shows the procedure of a new node generation. The new coin is placed into the domain surrounded by the closed node-chain. The new coin may be tangential to the chosen adjacent coins, or the radius of the new coin, r_A, may be given by the user or defined by system defaults; 4) Connect relevant nodes to form a new element, as in Figure 6, and then modify the advancing front node-chain by inserting N_A into the chain. 5) Go back to the third step. If the node-chain has only three nodes left, triangulate them directly.

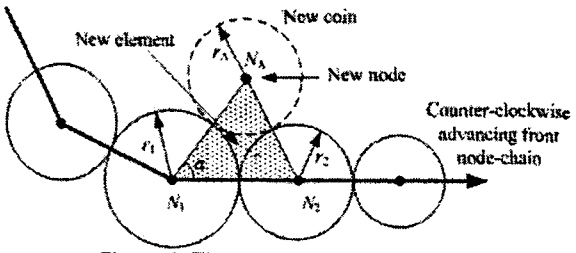

Figure 6: The new node N_A generation

With this mesh generation method, a reasonable mesh is produced. Considering adaptive refinement, the radius of a coin in the region, in which the error of finite element is greater than the desired permissive error, may be calculated with the refinement factor which is deduced by the fuzzy controller described as in the next section.

3.2. Fuzzy Control Adaptive Strategy

In this paper, the Zienkiewicz-Zhu error estimator is applied. In some cases, such as nonlinear problem, the relationship between the new refining element size and the error is difficult to construct.

As to the fuzzy control theory, the input parameter of the fuzzy controller of adaptive refinement is the error of element, denoted with linguistic variable set E. The output is refinement factor of element size, represented by linguistic variable set U. Positive large (PL), positive medium (PM), positive small (PS), zero (ZR), negative small (NS), negative medium (NM), and negative large (NL) are terms of the linguistic variables E and U.

According to the experience and the requirement for FEM calculation, the sense rules are established based on the following principle: if the error is greater than the desired permissive error, the size of the element should be reduced. The greater the difference is, the more the reduction. The fuzzy controller can be expressed as a set of fuzzy linguistic rules as follows:

If $E - E_0 = PL$ then $U = NL$,
If $E - E_0 = PM$ then $U = NM$,
If $E - E_0 = PS$ then $U = NS$,
If $E - E_0 = ZR$ then $U = ZR$,
If $E - E_0 = NS$ then $U = PS$,
If $E - E_0 = NM$ then $U = PM$,
If $E - E_0 = NL$ then $U = PL$,

where E_0 is the linguistic variable set of desired permissive error.

The universe of discourse for input and output variables is chosen as

$$X = \{-5 \quad -4 \quad -3 \quad -2 \quad -1 \quad 0 \quad 1 \quad 2 \quad 3 \quad 4 \quad 5\}$$

The membership function is a normal distribution expressed as

$$\mu(x)=\frac{(e^{-\frac{(x+5)^2}{2}})}{-5}+\frac{(e^{-\frac{(x+4)^2}{2}})}{-4}+\frac{(e^{-\frac{(x+3)^2}{2}})}{-3}+\frac{(e^{-\frac{(x+2)^2}{2}})}{-2}+\frac{(e^{-\frac{(x+1)^2}{2}})}{-1}+\frac{(e^{-\frac{x^2}{2}})}{0}+\frac{(e^{-\frac{(x-1)^2}{2}})}{1}+\frac{(e^{-\frac{(x-2)^2}{2}})}{2}+\frac{(e^{-\frac{(x-3)^2}{2}})}{3}+\frac{(e^{-\frac{(x-4)^2}{2}})}{4}+\frac{(e^{-\frac{(x-5)^2}{2}})}{5} \quad (1)$$

The fuzzy relation R contains a set of fuzzy sense rules is shown as

$$R=\bigcup_{i=1}^{7} R_i=\bigcup_{i=1}^{7}(E_i\times U_i)$$

The output U depending on the input E can be described as the following converting equation

$$U=E\circ R$$

where ' $\circ$ ' is an operator of fuzzy logic.

After the output U is solved based on the established control rules, the Centre of Area (COA) is employed as the reasoning method for the defuzzification of the output U to achieve refinement factor.

3.3. Application of Fuzzy Control Adaptive FE Meshing

Figure 7 is a cross-sectional diagram of a permanent magnet brushless DC (BLDC) motor. The shaded area represents permanent magnets. In a study of the influence of cogging torque, the effect of stator winding can be ignored.

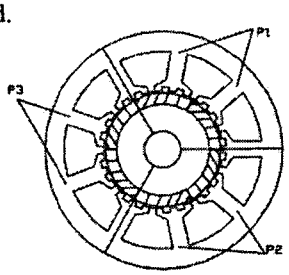

Figure 7: Structure of a permanent magnet BLDC motor

The initial mesh and magnetic field distribution are shown in Figure 8 with 13.7% error. After two refining iteration, the final adapted mesh and magnetic field distribution are shown in Figure 9 with 4.8% error. In Figure 9 the elements, which are near to air-gap, equivalent currents of permanent magnets and the points P_1, P_2 and P_3, are refined, respectively. The magnetic field distribution in Figure 9 is much smoother than that in Figure 8.

4. Field-Circuit Coupled Transient Computation

4.1. The Improved V-A Characteristic of Ideal Switches

Generally, the traditional V-A relationship of ideal diode in Figure 10(a) is:

$$\left.\begin{array}{ll} u=0, & i=0 \\ u=0 & i>0 \\ i=0 & u<0 \end{array}\right\} \quad (2)$$

where u is the applied voltage across the diode, and i is the current through the diode.

Because at least one of u and i equals 0, in the case of values, the system of (2) can be improved as the following single equation.

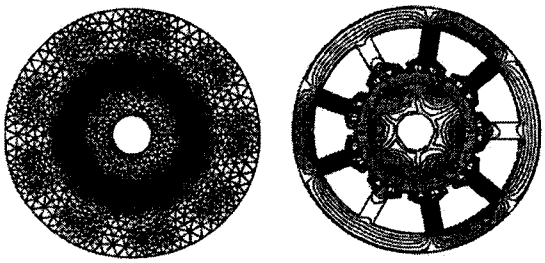

Figure 8: Initial mesh and associated distribution of magnetic field (3610 nodes / 7677 elements).

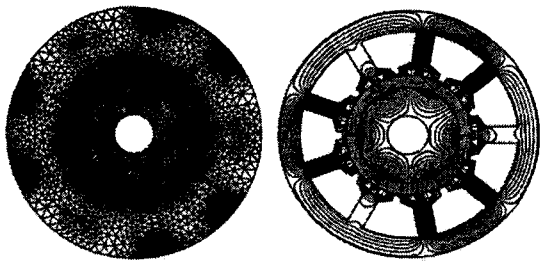

Figure 9: Adapted mesh and associated distribution of magnetic field (8006 nodes / 15698 elements).

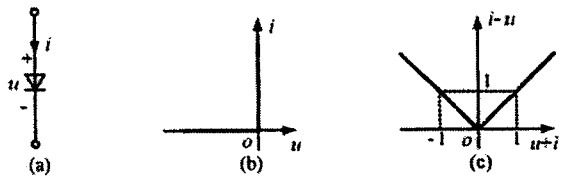

Figure 10: The conventional and improved V-A characteristics of an ideal diode: (a) an ideal diode, (b) the conventional V-A characteristic, and (c) the improved V-A characteristic.

$$u-i+\mathrm{abs}(u+i)=0 \quad (3)$$

The corresponding improved characteristic is illustrated in Figure 10(c).

By (3), the open-circuit or short-circuit states of a diode can be determined automatically. The circuit equations can be constructed with only one topology.

In the same way, the V-A relationship of ideal voltage controlled switches is expressed as (4). Equation (5) is the V-A relationship of ideal current controlled switches.

$$(u-i)+(u+i)\mathrm{sgn}(u_C-V_T)=0 \quad (4)$$

$$(u-i)+(u+i)\mathrm{sgn}(i_C-I_T)=0 \quad (5)$$

In (4) and (5), sgn(x) is a signum function, u is the voltage across the switch, i is the current through the switch, u_c is a controlling voltage, V_T is the threshold voltage, i_c is a controlling current, and I_T is the threshold current.

4.2. The Field-Circuit Coupled Transient Model

Disregarding the eddy current in the filament conductors, the 2-dimensional magnetic field model is described as:

$$\nabla\cdot(\nu\nabla A)+\nu\left(\frac{\partial M_y}{\partial x}-\frac{\partial M_x}{\partial y}\right)+\frac{d_f N_f}{S_f a}i_z=0 \quad (6)$$

where A is the Z-axis component of vector magnetic potential, ν magnetic reluctivity, M the magnetization of the permanent magnet, N_f the total conductor numbers of one winding in a slot, d_f the polarity (+1 or -1) to represent the forward path and return path of windings, S_f area of one slot; a the number of parallel branches in one winding; and i_s the current of this stranded stator winding.

By Galerkin triangular FE formulation, (6) can be discretized and expressed as a matrix equation:

$$\boldsymbol{KA}-\boldsymbol{DI}_{\mathrm{W}}=\mathbf{0} \tag{7}$$

where $\boldsymbol{K}$ is stiffness matrix, $\boldsymbol{A}$ denotes the column vector of vector magnetic potentials; $\boldsymbol{I}_{\mathrm{w}}$ current vector of winding conductors, $D_{ik}=\dfrac{d_f N_f}{S_{f_k} a}\int_{S_k}\beta_i dS$, β_i is the element shape function.

The voltage drop, u_s, in the winding is

$$\frac{d\psi_f}{dt}+l_e\frac{di_s}{dt}+R_f i_s=u_s \tag{8}$$

where, l_e the leakage inductance of the end winding, i_s the current through the winding; ψ_f is the flux-linkage associated with winding, and R_f the total resistance of the winding. Equation (8) can be expressed as

$$\frac{p}{a}\sum_{1}^{N_w}\frac{d_f N_f l}{S_f}\iint_{S_f}\frac{\partial A}{\partial t}dS+l_e\frac{di_s}{dt}+R_f i_s=u_s \tag{9}$$

where N_w is the slot number of the winding in the solution area; p is the ratio of the full cross-sectional area to the solution area, l the axial slot length.

Equation (9) can be expressed as the following matrix equation:

$$-\boldsymbol{GpA}-\boldsymbol{RI}_{\mathrm{W}}-\boldsymbol{L}_e p\boldsymbol{I}_{\mathrm{W}}+\boldsymbol{A}_{\mathrm{W}}^{\mathrm{T}}\boldsymbol{U}_n=\mathbf{0} \tag{10}$$

where, $\boldsymbol{G}$ is coefficient matrix of vector magnetic potential $\boldsymbol{A}$, $\boldsymbol{L}_e$ is diagonal matrix of leakage inductances of the end-windings; $\boldsymbol{R}$ is diagonal matrix of winding resistance, $\boldsymbol{U}_{\mathrm{n}}$ the vector of nodal voltage, and p the differential operator, $\boldsymbol{A}_{\mathrm{w}}$ the node-branch incidence matrix of the windings.

Considering the eddy current in the solid conductors, the governing equation of magnetic field is

$$\nabla\cdot(\nu\nabla A)-\sigma\frac{\partial A}{\partial t}+\frac{d_f\sigma}{l}u_{bar}=0 \tag{11}$$

where u_{bar} is the voltage between the two terminals of a solid conductor, σ conductivity of materials.

The circuit equation of a branch of the solid conductor is described as

$$\frac{d_f l}{S_{bar}}\iint_{S_{bar}}\frac{\partial A}{\partial t}dS_{bar}+R_{bar}i_{bar}-u_{bar}=0 \tag{12}$$

where, i_{bar} is the current trough the solid conductor, R_{bar} is the resistance of the solid conductor, S_{bar} the cross-sectional area of the solid conductor, $R_{bar}=l/(\sigma S_{bar})$.

The matrix of (12) is similar to (10). By substituting (12) into (11), one can obtain

$$\nabla\cdot(\nu\nabla A)-\sigma\frac{\partial A}{\partial t}+\frac{d_f}{S_{bar}}d_f\sigma\iint_{S_{bar}}\frac{\partial A}{\partial t}dS+\frac{d_f}{S_{bar}}i_{bar}=0 \tag{13}$$

The Galerkin triangular FE formulation of (13) is expressed as

$$\boldsymbol{KA}+\boldsymbol{TpA}-\boldsymbol{FI}_{\mathrm{bar}}=\mathbf{0} \tag{14}$$

where, p is the differential operator, $\boldsymbol{T}$ the coefficient matrix of differential of $\boldsymbol{A}$, $\boldsymbol{F}$ the the coefficient matrix of differential of current $\boldsymbol{I}_{\mathrm{bar}}$.

In this paper, the MNA is employed to describe the single general topology of a power electronics circuit.

The corresponding MNA equations are expressed as:

$$\begin{bmatrix}A_w\begin{bmatrix}I_w\\0\end{bmatrix}+\begin{bmatrix}A_{bar}\end{bmatrix}\begin{bmatrix}I_{bar}\\0\end{bmatrix}+\begin{bmatrix}Y_{n1}&A_2\\Y_2A_2^{\mathrm{T}}&Z_2\end{bmatrix}\begin{bmatrix}U_n\\I_2\end{bmatrix}+\begin{bmatrix}Y_{nc}&0\\0&-L\end{bmatrix}p\begin{bmatrix}U_n\\I_2\end{bmatrix}+\\ \begin{bmatrix}A_D\end{bmatrix}\begin{bmatrix}I_D\\0\end{bmatrix}+\begin{bmatrix}A_S\end{bmatrix}\begin{bmatrix}I_S\\0\end{bmatrix}=\begin{bmatrix}I_{s1}\\E_2\end{bmatrix}\end{bmatrix} \tag{15}$$

where, $\boldsymbol{A}_{\mathrm{bar}}$, $\boldsymbol{A}_2$, $\boldsymbol{A}_{\mathrm{D}}$, **and** $\boldsymbol{A}_{\mathrm{S}}$ are the node-branch incidence matrices of the solid conductors, voltage sources, diodes and switches, respectively; p denotes the differential operator; $\boldsymbol{Y}_{n1}$ is the nodal admittance matrix and $\boldsymbol{Y}_{nc}$ is the nodal capacitance matrix; $\boldsymbol{Y}_2\boldsymbol{A}_2^{\mathrm{T}}$, $\boldsymbol{Z}_2$, $\boldsymbol{L}$ are the corresponding V-A relationship matrices of voltage source branches and inductance branches; $\boldsymbol{U}_n$ the nodal voltage vector; $\boldsymbol{I}_2$ the current vector of voltage sources and inductances; $\boldsymbol{I}_{s1}$ the vector of independent current sources; $\boldsymbol{E}_2$ the vector of independent voltage sources; $\boldsymbol{I}_{\mathrm{D}}$ and $\boldsymbol{I}_{\mathrm{S}}$ are the current vectors of diodes and switches respectively.

According to the MNA, the V-A characteristic equations of each diode and each switch have been taken into account.

$$u_{nDi}-u_{nDj}-i_{D_k}+\mathrm{abs}\left(u_{nDi}-u_{nDj}+i_{D_k}\right)=0 \tag{16}$$

$$\left(u_{nSi}-u_{nSj}-i_{S_k}\right)+\left(u_{nSi}-u_{nSj}+i_{S_k}\right)\mathrm{sgn}\left(u_C-V_T\right)=0 \tag{17}$$

where, i_{D_k} and i_{S_k} are the current through the diode and switch, respectively, $(u_{nDi}-u_{nDj})$ and $(u_{nSi}-u_{nSj})$ are the voltage across the diode and switch, respectively.

The mechanical equation governing the rotor motion is:

$$J_m\frac{d\omega}{dt}=T_e-T_f \tag{18}$$

where J_m is the moment of inertia, ω is the rotor speed, T_e is the electromagnetic torque, and T_f is the load torque. Maxwell stress tensor method is used for torque computation.

The coupling between rotor and stator can be tackled with a band in the air gap. The band being re-meshed is required in each time step. To avoid the badly formed elements, the Delaunay optimal approach is adopted to improve the element quality. The backward Euler's method is applied to discretize the time variables and the Newton-Raphson method is used for nonlinear problem.

4.3. Application of Field-Circuit Transient Computation

The proposed method has been used to simulate the performance of a permanent magnet brushless DC motor with an external rotor. The rotor steel shell is laminated. The number of turns per slot is 24. Figure 11 shows the model of the BLDC motor and its drive circuit, which comprises the 3-phase bridge inverter using a six-MOSFET module, and a 120° conduction controller. The simulating process is assumed that the BLDC motor starts from a speed of 0 and a load of 6.6 Nm. After 0.2 s, the load torque is reduced to 0.46 Nm. The simulating results of phase current, rotor speed and torque are shown in Figure 12, respectively.

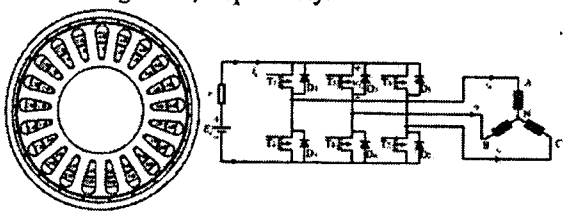

Figure 11: A BLDC motor and its drive circuit

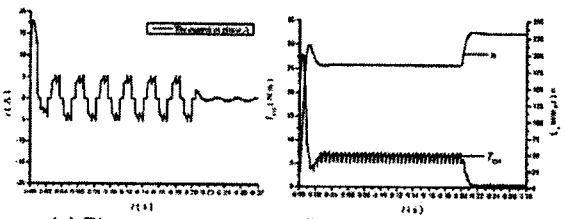

(a) Phase current (b) speed and torque

Figure 12: Some simulation results

When the motor is operating steadily, the simulation and experiment results of phase current are shown in Figure 13, respectively. At this time, the load torque is 6.6 Nm. Figure 14 shows the simulation and experimental voltage of switch T_3, respectively.

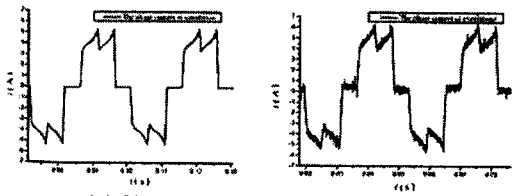

(a) Simulation (b) Experiment

Figure 13: Phase current with a torque of 6.6Nm

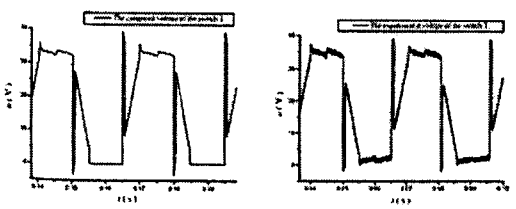

(a) Simulation (b) Experiment

Figure 14: Voltage of T_3 with a torque of 6.6 Nm

5. Conclusions

This paper introduced the parameterized FE geometric modelling, fuzzy control adaptive meshing and field-coupled computation considering power electronics in a developed FE package.

Petri net provides a clear description for parametric modelling, which can avoid the complexity of calculating the nonlinear equations in variational geometry, and easily find out potential conflict constraints. The user may define the parametric FE model in diverse order due to the constraint reasoning being independent of modelling sequence.

The fuzzy control meshing can provide a reasonable mesh distribution. The approximate relationship between error and refinement factor has been deduced. A fine mesh, which satisfies precision requirements, can be obtained with fewer refinement iterations. Thus, this adaptive meshing exhibits higher efficiency. Advantages of the proposed method are manifested in its applications in some electromagnetic problems.

An improved V-A characteristic of ideal switch and diode have been presented, and applied to the coupled magnetic field with power electronics circuit simulation. It is found that the circuit equations can be constructed with only one topology, and the switch states can be detected automatically. It is convenient for the realization of versatile simulation package. From the simulation and experimental results, it can be seen that the improved coupled field-circuit simulation is accurate.

The future work focuses on the 3D FE calculation and web-based FE analysis.

References

[1] Wang Shuhong, Qiu Jie, and Qingfu Li, "A New Parametric Finite Element Modeling Technique Based on Petri Net," Proceedings of Asian Symposium on Applied Electromagnetics, pp119-122, 2001.

[2] Shuhong Wang, Liang Yuan, Jie Qiu, and Semyung Wang, "Feature-based Fuzzy Control Adaptive Finite-element Mesh Generation for Electromagnetic Fields," IEEE Trans. on Magnetics, vol. 41, no. 5, pp1688-1691, 2005.

[3] Shuhong Wang, Luhuai Zhao, Jie Qiu, Qingfu Li, Xinghua Wang, and Qunfeng Li, "An Improved V-A Characteristics of Switches and Its Application in Coupled Field-circuit Simulation of Permanent Magnet Brushless DC Motor," Proceedings of International Conference on Power Electronics and Motor Control, vol. 2, pp1013-1017, 2004.

[4] C.F. Parker, J.K. Sykulski, and S.C. Taylor, "Parametric Environment for EM Computer Aided Design," IEEE Trans. on Magnetics, vol.33 , no. 3, pp1433-1436, 1996.

[5] U. Pahner, R. Mertens, H. D. Gersem, R. Belmans, and K. Hameyer, "A Parametric Finite Element Environment tuned for Numerical Optimization," IEEE Trans. on Magnetics, vol.34, no.5, pp 2936-2939, 1998.